Manipulating matter rogue waves and breathers in Bose-Einstein condensates

K. Manikandan,[1] P. Muruganandam,[2] M. Senthilvelan,[1] and M. Lakshmanan[1]
[1]*Centre for Nonlinear Dynamics, Bharathidasan University, Tiruchirappalli 620024, Tamilnadu, India*
[2]*Department of Physics, Bharathidasan University, Tiruchirappalli 620024, Tamilnadu, India*
(Received 2 July 2014; revised manuscript received 17 September 2014; published 2 December 2014)

We construct higher-order rogue wave solutions and breather profiles for the quasi-one-dimensional Gross-Pitaevskii equation with a time-dependent interatomic interaction and external trap through the similarity transformation technique. We consider three different forms of traps: (i) the time-independent expulsive trap, (ii) time-dependent monotonous trap, and (iii) time-dependent periodic trap. Our results show that when we change a parameter appearing in the time-independent or time-dependent trap the second- and third-order rogue waves transform into the first-order-like rogue waves. We also analyze the density profiles of breather solutions. Here we also show that the shapes of the breathers change when we tune the strength of the trap parameter. Our results may help to manage rogue waves experimentally in a BEC system.

DOI: 10.1103/PhysRevE.90.062905 PACS number(s): 05.45.Yv, 03.75.Kk, 03.75.Lm, 67.85.Hj

I. INTRODUCTION

During the past several years considerable interest has been shown in exploring localized nonlinear waves in the variable coefficient nonlinear Schrödinger (NLS) equation and its generalizations [1–3]. The motivation comes from the fact that NLS equation and its variants appear in several branches and topics of physics, including nonlinear optics [4,5] and Bose-Einstein condensates (BECs) [6–8], etc. Focusing our attention on BECs alone, it is well known that the Gross-Pitaevskii (GP) equation governs the evolution of macroscopic wave function at ultra-low temperatures [6,9]. In particular, for cigar-shaped BECs, it has been shown that the GP equation can be reduced to the one-dimensional variable coefficient NLS equation [10–12]

$$i\psi_t + \tfrac{1}{2}\psi_{xx} + R(t)|\psi|^2\psi + \tfrac{1}{2}\beta(t)^2x^2\psi = 0, \qquad (1)$$

where $\psi(x,t)$ is the condensate wave function, t is the dimensionless normalized time, x is the dimensionless normalized coordinate in the axial direction, $R(t)$ represents the effective scattering length, and $\beta(t)$ is the axial trap frequency.

A simple and straightforward way of exploring the localized and periodic structures of (1) is by transforming it into a constant coefficient NLS equation through a suitable transformation. From the known solutions of the latter equation the solutions of the former equation can be identified. Using this procedure a class of solutions, in particular various localized solutions, have been identified for the model (1), including soliton, breather, and rogue wave (RW) solutions. In order to appreciate the relevance of the above type of localized structures for Eq. (1), we may first consider their existence in the case of a constant coefficient NLS equation,

$$iU_T + \tfrac{1}{2}U_{XX} + |U|^2U = 0. \qquad (2)$$

It is well known that the standard NLS equation (2) admits the following basic localized profiles and their higher-order versions [13].

(i) *Envelope soliton:* It is a solitary wave (localized envelope along with a carrier wave) that retains its characteristics (amplitude, shape and velocity) under collision with another soliton, except for a change in phase. The intensity profile of the soliton is shown in Fig. 1(a). The typical form of the envelope soliton is

$$U(X,T) = P_{1R}\exp^{i\eta_1}\operatorname{sech}\eta_2, \qquad (3)$$

where $P_1(=P_{1R}+iP_{1I})$ is a complex constant, $\eta_1 = P_{1I}X + [(P_{1R}^2 - P_{1I}^2)T]/2 + \eta_{1I}^{(0)}$, and $\eta_2 = P_{1R}(X - P_{1I}T) + \eta_{1R}^{(0)} + \log(1/2P_{1R})$. Here $\eta_{1R}^{(0)}$ and $\eta_{1I}^{(0)}$ are constant parameters.

(ii) *Breather:* It is a localized solution with temporally and/or spatially periodic structures having constant background exhibiting internal oscillations and bound states of nonlinear wave packets [14], which is represented in Fig. 1(b). Its typical form reads [15]

$$U(X,T) = \rho_0\cos(2\phi_R)\exp i(\theta+2\phi_R)\Bigg(1+\frac{1}{\sqrt{a}\cosh(\eta_R+\sigma)+\cos\eta_I} \times\left\{\left(\frac{\cosh 2\phi_I}{\cos 2\phi_R}-1\right)\cos\eta_I + i\left[\tan 2\phi_R\sinh(\eta_R+\sigma) - \frac{\sinh 2\phi_I}{\cos 2\phi_R}\sin\eta_I\right]\right\}\Bigg), \qquad (4)$$

where ρ_0 is the amplitude of the plane wave, $\theta = kX - \omega T$, σ, k, ω are constant parameters, $\eta_R = P_RX - (\Omega_RT)/2 + \eta_R^0$, $\eta_I = P_IX - (\Omega_IT)/2 + \eta_I^0$, $\Omega_R = 2kP_R - \frac{P_R^2-P_I^2\sin 2\phi_R+2P_RP_I\sinh 2\phi_I}{\cosh 2\phi_I-\cos 2\phi_R}$, $\Omega_I = 2kP_I + \frac{P_R^2-P_I^2\sin 2\phi_I+2P_RP_I\sinh 2\phi_R}{\cosh 2\phi_I-\cos 2\phi_R}$, $a = \cosh^2\phi_I/\cos^2\phi_R$, $P_R = -2\rho_0\cos\phi_R\sinh\phi_I$, $P_I = 2\rho_0\sin\phi_R\cosh\phi_I$, and $\phi = \phi_R + i\phi_I$ is a complex constant. This solution is also called a general breather (GB) since it is periodic both in space and in time. Two important special cases are the following: (i) When $\phi_R \neq 0$ and $\phi_I = 0$, the GB solution corresponds to an Akhmediev breather (AB), which is periodic in space

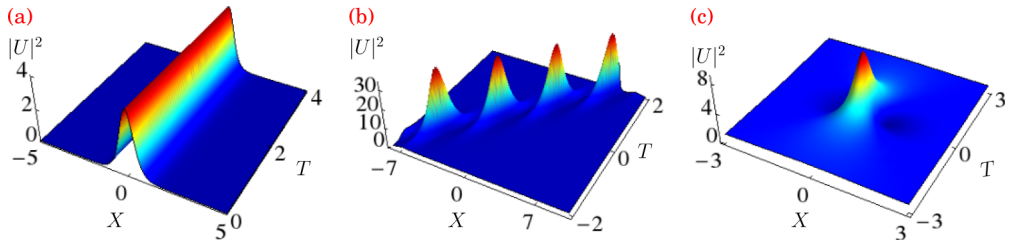

FIG. 1. (Color online) Profiles of (a) soliton, (b) general breather, and (c) Peregrine soliton (rogue wave).

and localized in time. (ii) If we take $\phi_R = 0$ and $\phi_I \neq 0$, (4) becomes a Ma breather (MB) which is periodic in time only and localized in space.

(iii) *Rogue wave:* A further specialized structure, which is localized both in space and in time with a constant plane wave background, is the so-called Peregrine soliton or RW [16]. It can be obtained by taking the limits $\phi_R = \epsilon\gamma$ and $\phi_I = \epsilon\delta$, and $\epsilon \to 0$, where γ, δ and ϵ are constants. Then Eq. (4) reduces to the following form:

$$U(X,T) = \rho_0\, e^{i\theta}\left[1 - \frac{4 + 8i\rho_0^2 T}{1 + 4\rho_0^2(X - kT)^2 + 4\rho_0^4 T^2}\right]. \quad (5)$$

Very often the above localized nonlinear wave is described as a wave that "appears from nowhere and disappears without a trace" [17], as shown in Fig. 1(c). It was first observed in the area of oceanography [18] and is traditionally defined as a wave whose wave height (the distance from trough to crest) is more than twice the significant wave height. The latter is generally defined as the average wave height among one third of highest waves in a given time series [18,19]. Further, it has also been explained that the above structure (5) arises due to a modulation instability) [16,20] of the plane wave solution of the constant coefficient NLS equation. Very recently higher-order RWs (HRWs) which correspond to the higher-order rational solutions of the NLS equation (2) have been deduced [21]. The explicit expressions for the second- and third-order RWs of the NLS equation are given in the Appendix. These HRWs have higher amplitudes than the first-order RW. The RWs have also been observed experimentally in physical systems such as water wave tanks [22], capillary waves [23], and nonlinear optics [5,24]. Several theoretical studies on the dynamics of RWs in nonlinear fiber optics [25,26], plasma physics [27], laser-plasma interactions [28], and even econophysics [29], described by a scalar NLS equation, have been made recently.

Now, as mentioned at the beginning, the dynamics of a cigar-shaped BEC at absolute zero temperature is usually described by the mean-field GP equation (1), which is a generalized form of the ubiquitous constant coefficient NLS equation (2), for the wave function of the condensate. Since the NLS equation (2) admits breather and RW solutions, it is natural to expect that RWs and breathers may also be found in BEC systems as well. In this context, the RWs can correspond to a sudden increase of peaks in the condensate clouds similar to the nature of high peaks in the open sea, while breathers are generalizations of the RWs. The formative mechanism for the matter RWs in BECs is the accumulation of energy and atoms towards its central part and their spreading out to a constant density background. The formation of matter breather is the periodic exchange of atoms between the profile and the plane wave background. From an experimental point of view, the existence of RW and breather structures in a BEC system can be effectively controlled by tuning the nonlinear interaction between atoms by Feshbach resonance technique [7,30,31] and modulating the trapping frequency of the external potential. It will therefore be of great interest to study the characteristics and/or controlling of structures of RWs and breathers due to their localization both in space and in time in BEC experiments. Past explorations of the GP equation in BECs have paved the way for important developments in manipulating coherent matter waves for application, including atom interferometry [32], coherent atom transport [33], and quantum information processing or quantum computation [34]. Therefore, it is of high significance to study the dynamics of RWs and breather profiles of the GP equation (1). However, only a few attempts have been made to identify and analyze the RWs and breather solutions of (1) [35–40]. To the best of our knowledge neither higher-order RW solutions (with certain free parameters) nor higher-order breather solutions of (1) have been taken up for study. Motivated by these observations, in this work we construct the aforementioned localized and periodic solutions of (1). Besides constructing these two families of solutions we also investigate how to manipulate the RWs and breathers through the effective scattering length and the strength of the trap parameter.

Having stated our motivation we now proceed to construct a transformation that transforms Eq. (1) into the standard NLS equation (2). Following the standard procedure [11,41] we find that the required similarity transformation should be of the form

$$\psi(x,t) = r_0\sqrt{R(t)}[U(X,T)] \times \exp\left\{i\left[c_1 r_0^2 R x - \frac{R_t}{R}x^2 - \frac{1}{2}c_1^2 r_0^4 \int R^2(t)\,dt\right]\right\}, \quad (6)$$

where

$$X(x,t) = r_0 R(t)x - c_1 r_0^3 \int R^2(t)\,dt, \quad (7a)$$

$$T(t) = r_0^2 \int R^2(t)\,dt, \quad (7b)$$

and $U(X,T)$ is the solution of the standard NLS equation (2). In the above b, r_0 are arbitrary constants, and the modulational functions $R(t)$ and $\beta(t)^2$ should satisfy the following condition:

$$\frac{d}{dt}\left(\frac{R_t}{R}\right) - \left(\frac{R_t}{R}\right)^2 + \beta(t)^2 = 0, \quad (8)$$

which is a Riccati-type equation with dependent variable (R_t/R) and independent variable t. Regardless of what $R(t)$ is, as long as condition (8) is satisfied, the GP equation is integrable [11,41]. We also note here that the Painlevé singularity structure analysis performed on Eq. (1) confirms the same restriction (8) on the system coefficients [42]. We further note that solution (6) provides us some flexibility to generate new structures related to the RWs, which may be useful for the BEC experiments.

Even though one can arbitrarily choose the functions $R(t)$ and $\beta(t)$ that satisfy the constraint (8) and generate the required solutions, in this paper we consider the trap frequency to be of the following three forms: (i) $\beta(t)^2 = \beta_0^2$, (ii) $\beta^2(t) = (\beta_0^2/2)[1 - \tanh(\beta_0 t/2)]$, and (iii) $\beta(t)^2 = 2\beta_0^2[1 + 3\tan^2(\beta_0 t)]$, where β_0 is a constant. As shown in Ref. [11] the effective scattering length for these three cases turns out to be (i) $R(t) = \mathrm{sech}\,(\beta_0 t + \delta)$, (ii) $R(t) = 1 + \tanh(\beta_0 t/2)$, and (iii) $R(t) = 1 + \cos(2\beta_0 t)$. We consider the trap frequency to be in the above forms since it has been shown that they are valid forms in BEC experiments [11]. We consider each one of the cases separately and substitute them in Eq. (6) along with the RW and breather solutions of (2). We then analyze in detail how the nature of the RW and breather structures get modified by the above two functions $\beta(t)$ and $R(t)$. Our analysis shows that the amplitude parameter (r_0) plays a vital role in the formation of RWs, and the trap frequency and the effective scattering length modify the structure of the RW and breather profiles, allowing one the possibility of manipulating the RWs and breathers in specific ways.

The paper is organized as follows. In the following section, we construct RW solutions for time-independent and time-dependent traps and study their characteristics in detail. We observe that the second- and third-order RWs transform to first-order RW-like structures when we tune a parameter which appears in the harmonic traps (time-independent and time-dependent traps). In Sec. III, we also construct RW solutions with free parameters which allow us to split the symmetric form solution into a multipeaked solution for (1) and investigate how these RW structures get modified in the plane wave background by increasing the strength of the trap. In Sec. IV, we construct one-breather and two-breather solutions of (1) and investigate their characteristics when we alter the trap parameter. Finally, in Sec. V, we present a summary of the results and our conclusions.

II. CHARACTERISTICS OF ROGUE WAVES

To begin, we consider the case in which the trap frequency is a constant, that is, $\beta(t)^2 = \text{const} = \beta_0^2$. A time-independent trap frequency implies that the frequency does not change with time and space. We then consider the trap frequency to be time-dependent and investigate the associated RW solutions.

A. Time-independent trap

Substituting $\beta(t)^2 = \beta_0^2$ in the integrability condition (8), we find that the time-dependent interaction term should be of the form $R(t) = \mathrm{sech}\,(\beta_0 t + \delta)$, where δ is an integration constant. Plugging this expression in Eq. (6), we find

$$\psi_j(x,t) = r_0\sqrt{\mathrm{sech}(\beta_0 t + \delta)}\, U_j(X,T)\eta(x,t), \tag{9}$$

where

$$\eta(x,t) = \exp\left\{ i\left[c_1 r_0^2 \mathrm{sech}(\beta_0 t + \delta)x + \frac{\left(\beta_0^2 x^2 - c_1^2 r_0^4\right)\tanh(\beta_0 t + \delta)}{2\beta_0}\right]\right\},$$

and $U_j(X,T)$, $j = 1,2,3$, are the first-, second-, and third-order RW solutions of the NLS equation (2) whose explicit expressions are given in the Appendix [see Eqs. (A2), (A4), and (A5)]. Also $X(x,t)$ and $T(t)$ have the forms as given in Eqs. (7).

In Fig. 2 the first, second, and third columns represent the density profiles of the first-, second-, and third-order RWs obtained from (9). In this figure we present the formation of RWs in cigar-shaped BECs. In the context of BECs, it is the fluctuation in the density of atoms, localized in space and time, which is what we observe as RWs. For instance, consider the first-order RWs depicted in Figs. 2(a)–2(d). These may be interpreted as follows: Atoms in the condensate, initially at a constant density background, suddenly accumulate to form a hump towards the center of the condensate at finite time while leaving voids in the density which appear as troughs in the RWs, depending on the initial state. The crest and troughs reach their extrema as time progresses, and then the condensate atoms spread out so as to recover the constant density background in finite time, thus revealing the unstable nature of RWs. Further, by tuning the amplitude parameter r_0 in Eq. (9), we can visualize the formation and manipulation of RWs. For example, when we increase the amplitude parameter r_0 smoothly from 0.5 to 1.2, we can observe in Figs. 2(a)–2(d) the formation of more and more localized first-order RWs with increasing amplitude. At $r_0 = 1.2$ one can visualize a large amplitude wave which is sufficiently localized both in space and in time, which in turn confirms the formation of the first-order RW in BEC. The formation of second and third-order RWs is also demonstrated in Figs. 2(c)–2(l), respectively, for the same set of parameter values of r_0. From these figures we infer that the time-dependent nonlinear interaction between the atoms induces density fluctuations over the condensate, which gets more and more localized both in space and in time as we increase the order of the RW.

In order to confirm the existence of the RWs further, we have also performed a direct numerical simulation of (1) with the aid of the split-step Crank-Nicolson method using an initial wave function which is the same as the function (9) and with space step $dx = 0.01$ and time step $dt = 0.001$ [43]. In Fig. 3 we have presented the computer-generated density profile of the first-order RW and the corresponding contour plot with the parameters chosen as $r_0 = 1.2$, $c_1 = 0.01$, $\beta_0 = 0.1$, and $\delta = 0.01$, which are same as that of Fig. 2(d). One can easily observe a very good agreement between the numerical results and the analytical predictions for the emergence of the RWs. We have also verified numerically the presence of second- and third-order RWs of (1), replicating Figs. 2.

Next we demonstrate how these localized structures vary with respect to the trap parameter β_0. Figure 4 displays the

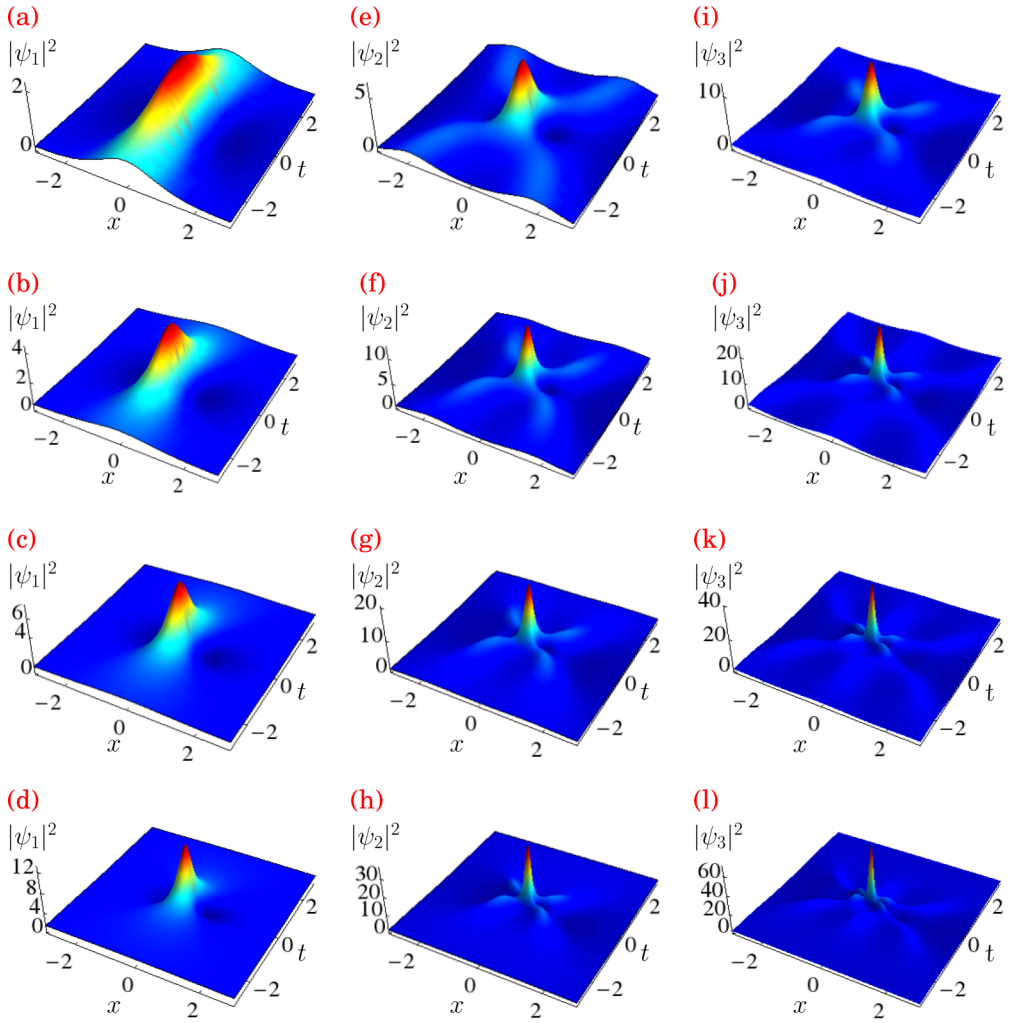

FIG. 2. (Color online) First, second, and third columns represent the formation of first-, second-, and third-order RWs in BECs for the time-dependent nonlinearity coefficient $R(t) = \mathrm{sech}(\beta_0 t + \delta)$ and time-independent trap frequency $\beta(t)^2 = \beta_0^2$, obtained using expression (9). The parameter $r_0 = 0.5$ for panels (a), (e), and (i), 0.7 for (b), (f), and (j), 0.9 for (c), (g), and (k), and 1.2 for (d), (h), and (l). The other parameters are $c_1 = 0.01$, $\beta_0 = 0.1$, and $\delta = 0.01$.

first-order RW for the same nonlinearity management parameter $R(t) = \mathrm{sech}(\beta_0 t + \delta)$ and the external trap frequency $\beta(t)^2 = \beta_0^2$. The nature of the first-order RW for $\beta_0 = 0.1$ is depicted in Fig. 4(a). When we increase the strength of the trap parameter the density profiles corresponding to the first-order RW become more and more localized in time as shown in Figs. 4(b) and 4(c), respectively. The corresponding contour plots are given in Figs. 4(d)–4(f).

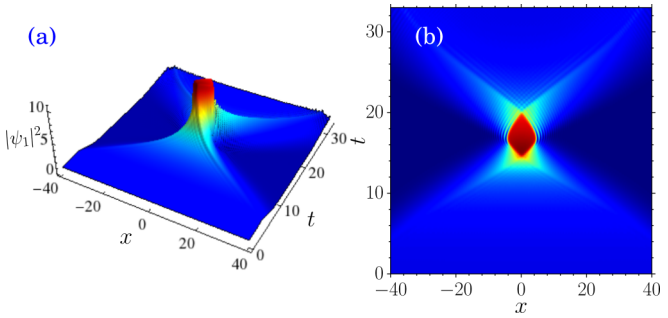

FIG. 3. (Color online) (a) First-order RW in BEC and (b) the corresponding contour plot obtained by numerically solving Eq. (1) through the split-step Crank-Nicolson method for the time-dependent nonlinearity coefficient $R(t) = \mathrm{sech}(\beta_0 t + \delta)$ and time-independent trap frequency $\beta(t)^2 = \beta_0^2$. The initial condition chosen corresponds to the analytic solution of Fig. 2(d).

Figure 5 displays the density profiles of the second-order RWs for the same nonlinearity management parameter as a function of β_0. In Fig. 5(a) we display the second-order RW for $\beta_0 = 0.1$. When the strength of the parameter β_0 is increased to 1.2, the wave subcrests start to stretch as shown in Fig. 5(b). The wave subcrests become more and more localized in time when we increase the value of β_0, and finally the second-order RW attains a new structure as given in Fig. 5(c) for $\beta_0 = 5.0$. The resultant structure looks almost like a first-order RW; see Fig. 4(c). Figures 5(d)–5(f) are the corresponding contour plots.

We also observe similar effects in the third-order RW case as well when we increase the value of β_0. Figure 6 demonstrates the changes in the third-order RW when we vary the interaction strength. At $\beta_0 = 1.5$, the third-order RW transforms into the second-order RW-like structure as shown in Fig. 6(b).

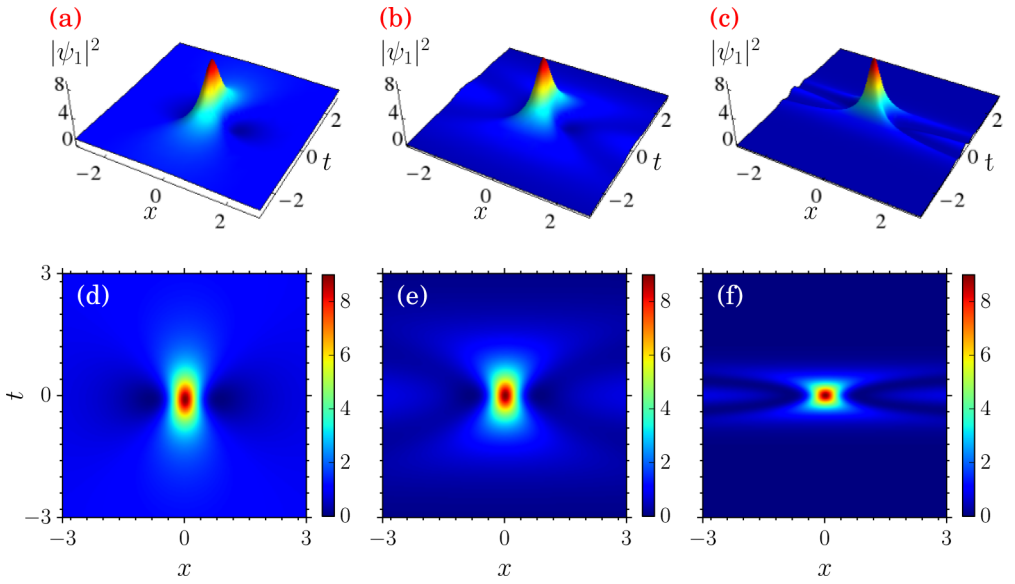

FIG. 4. (Color online) First-order RWs for $R(t) = \mathrm{sech}(\beta_0 t + \delta)$ and $\beta(t)^2 = \beta_0^2$. The parameter β_0 is varied as (a) $\beta_0 = 0.1$, (b) $\beta_0 = 1.2$, (c) $\beta_0 = 5.0$. Panels (d)–(f) are their corresponding contour plots. The other parameters are fixed as $r_0 = 1.0$, $c_1 = 0.01$, and $\delta = 0.01$.

When we increase the value of the parameter β_0 to 5.0, one obtains a first-order-like RW, which is displayed in Fig. 6(c). These facts are also confirmed by the corresponding contour plots, Figs. 6(d)–6(f). The aforementioned results reveal that when we increase the strength of the trap parameter β_0, the second- and third-order RWs become more localized in time and delocalized in space, approaching the structure of a first-order RW. Thus the robustness of the density profiles can be controlled by varying the strength of trap frequencies.

B. Time-dependent monotonous trap

Next we consider the time-dependent trap frequency in the form $\beta^2(t) = (\beta_0^2/2)[1 - \tanh(\beta_0 t/2)]$. For this choice, relation (8) fixes the interatomic interaction term to be of the form $R(t) = 1 + \tanh(\beta_0 t/2)$. The first-, second-, and third-order RW solutions for this trap frequency and strength of interatomic interaction are found to be

$$\psi_j(x,t) = r_0\sqrt{1 + \tanh\left(\frac{\beta_0}{2}t\right)}\, U_j(X,T)\, \eta(x,t), \tag{10}$$

where $j = 1,2,3$ and

$$\eta(x,t) = \exp\left[i\left(\frac{\beta_0 \mathrm{sech}^2\left(\frac{\beta_0 t}{2}\right)x^2}{4\left[1 + \tanh\left(\frac{\beta_0 t}{2}\right)\right]} - c_1 r_0^2\left[1 + \tanh\left(\frac{\beta_0 t}{2}\right)\right]x + \frac{c_1^2 r_0^4\left\{\beta_0 t + 2\log\left[\cosh\left(\frac{\beta_0 t}{2}\right) - \tanh\left(\frac{\beta_0 t}{2}\right)\right]\right\}}{\beta_0}\right)\right].$$

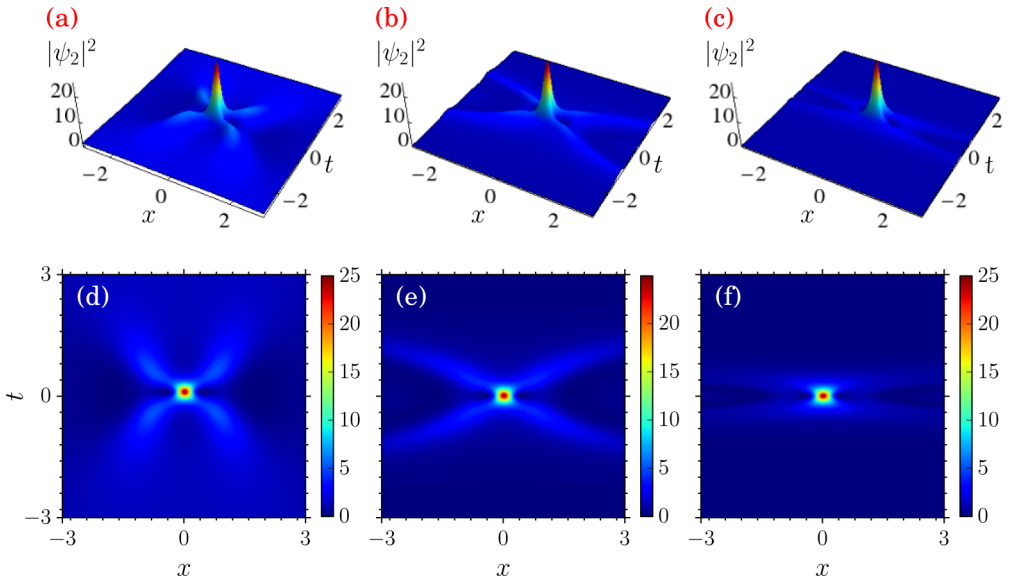

FIG. 5. (Color online) Second-order RWs for $R(t) = \mathrm{sech}(\beta_0 t + \delta)$ and $\beta(t)^2 = \beta_0^2$. The parameter β_0 is varied as (a)$\beta_0 = 0.1$, (b) $\beta_0 = 1.2$, (c) $\beta_0 = 5.0$. Panels (d)–(f) are their corresponding contour plots. The other parameters are the same as in Fig. 4.

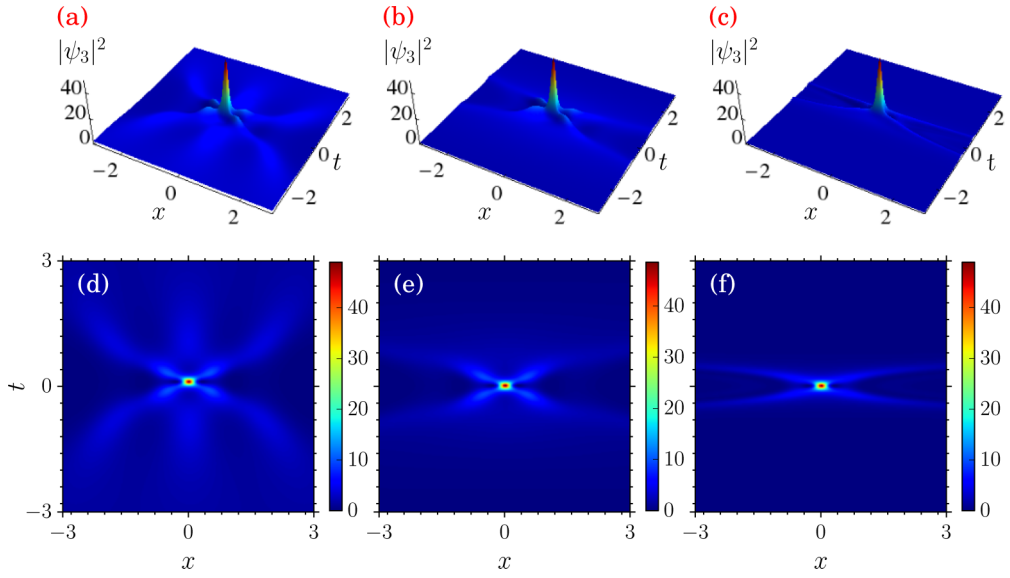

FIG. 6. (Color online) Third-order RWs for $R(t) = \mathrm{sech}(\beta_0 t + \delta)$ and $\beta(t)^2 = \beta_0^2$. The parameter β_0 is varied as (a) $\beta_0 = 0.1$, (b) $\beta_0 = 1.5$, (c) $\beta_0 = 5.0$. Panels (d)–(f) are their corresponding contour plots. The other parameters are the same as in Fig. 4.

The qualitative nature of the first-, second-, and third-order RWs for $R(t) = 1 + \tanh(\beta_0 t/2)$ and $\beta(t)^2 = \beta_0^2/2[1 - \tanh(\beta_0 t/2)]$ turns out to be the same as in the previous case [Figs. 2(d), 2(h), and 2(l)] when the amplitude parameter r_0 is varied, and so we do not display the outcome here separately. On the other hand, we identify interesting structures while varying the parameter β_0, which is discussed in the following.

In Fig. 7 we depict the first-order RW for these choices of $R(t)$ and $\beta(t)$. When $\beta_0 = 0.1$ the first-order RW is as shown in Fig. 7(a) [see also Fig. 7(d) for the corresponding contour plot]. By altering the value of the trap parameter β_0 to 1.0, the structure of the first-order RW gets modified as shown in Figs. 7(b) and 7(e). One can also see from Fig. 7 that, as the trap parameter β_0 is increased, the RW gradually becomes more localized in time and the condensate atoms settle down to a slightly higher density background due to the attractive nature of the potential. When $\beta_0 = 5.0$ the modified structure of the first-order RW is given in Figs. 7(c) and 7(f), where this feature is even more prominent. The density profiles of the corresponding second-order RWs are presented in Fig. 8. When we tune the parameter β_0 from 0.1 upwards the wave subcrests start to stretch. From the contour plots we can observe that the stretches occur on one side of the RW only. When we increase the value of β_0 further the second-order RW gets modified to a first-order RW-like structure, which is demonstrated in Fig. 8(c). A similar transition has also

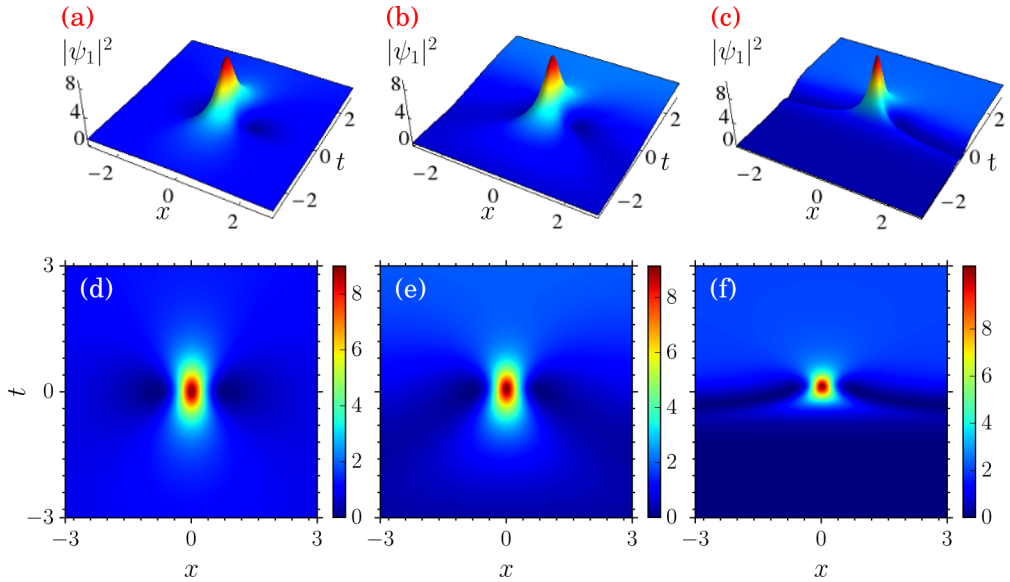

FIG. 7. (Color online) First-order RWs for $R(t) = 1 + \tanh(\beta_0 t/2)$ and $\beta(t)^2 = \beta_0^2/2[1 - \tanh(\beta_0 t/2)]$. The parameter β_0 is varied as (a) $\beta_0 = 0.1$, (b) $\beta_0 = 1.0$, and (c) $\beta_0 = 5.0$. Panels (d)–(f) are the corresponding contour plots of (a)–(c). The other parameters are the same as in Fig. 4.

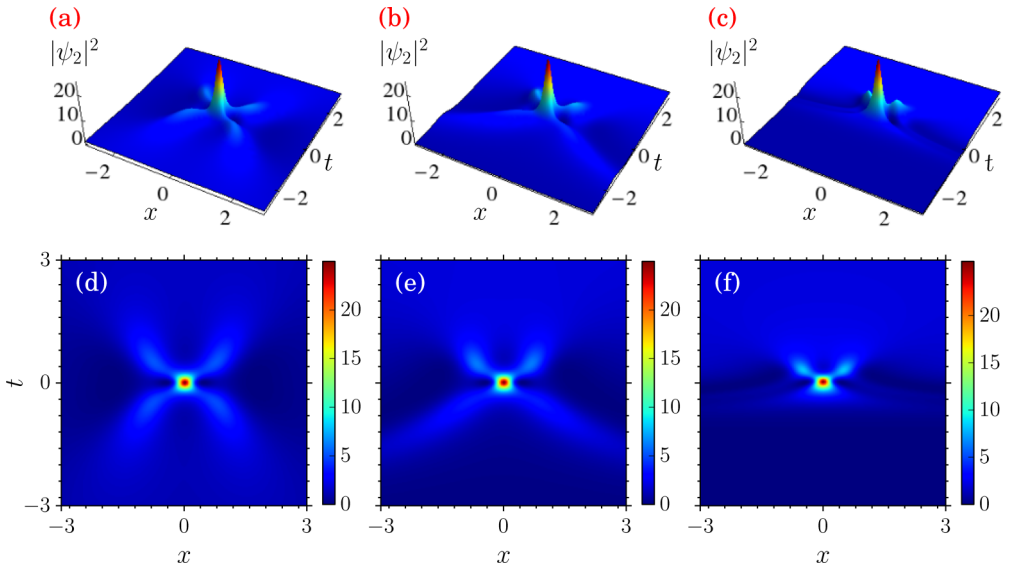

FIG. 8. (Color online) Second-order RWs for $R(t) = 1 + \tanh(\beta_0 t/2)$ and $\beta(t)^2 = \beta_0^2/2[1 - \tanh(\beta_0 t/2)]$. The parameter β_0 is varied as (a) $\beta_0 = 0.1$, (b) $\beta_0 = 1.0$, and (c) $\beta_0 = 5.0$. Panels (d)–(f) are the corresponding contour plots of (a)–(c). The other parameters are the same as in Fig. 4.

been observed in the third-order RW case as well, which is illustrated in Fig. 9. The third-order RW acquires a new structure as shown in Figs. 9(b) and 9(e) when we increase the value of the parameter β_0 from 0.1 to 1.0. At $\beta_0 = 5.0$, we observe that the third-order RW acquires a further modified structure which is displayed in Figs. 9(c) and 9(f). Note the similarity in the central part with that of the first-order RW as given in Figs. 7(c) and 7(f).

C. Time-dependent periodic trap

In the case of the third choice we consider the time-dependent periodic trap frequency to be of the form $\beta(t)^2 = 2\beta_0^2[1 + 3\tan^2(\beta_0 t)]$ so that the strength of the time-dependent periodic interatomic interaction turns out to be $R(t) = 1 + \cos(2\beta_0 t)$. Substituting these two expressions in Eq. (6), we find

$$\psi_j(x,t) = r_0\sqrt{1 + \cos(2\beta_0 t)}\, U_j(X,T)\, \eta(x,t), \tag{11}$$

where

$$\eta(x,t) = \exp\left(i\left\{\beta_0 \tan(\beta_0 t)x^2 + 2c_1 r_0^2 \cos(\beta_0 t)^2 x - \frac{c_1^2 r_0^4[12\beta_0 t + 8\sin(2\beta_0 t) + \sin(4\beta_0 t)]}{16\beta_0}\right\}\right).$$

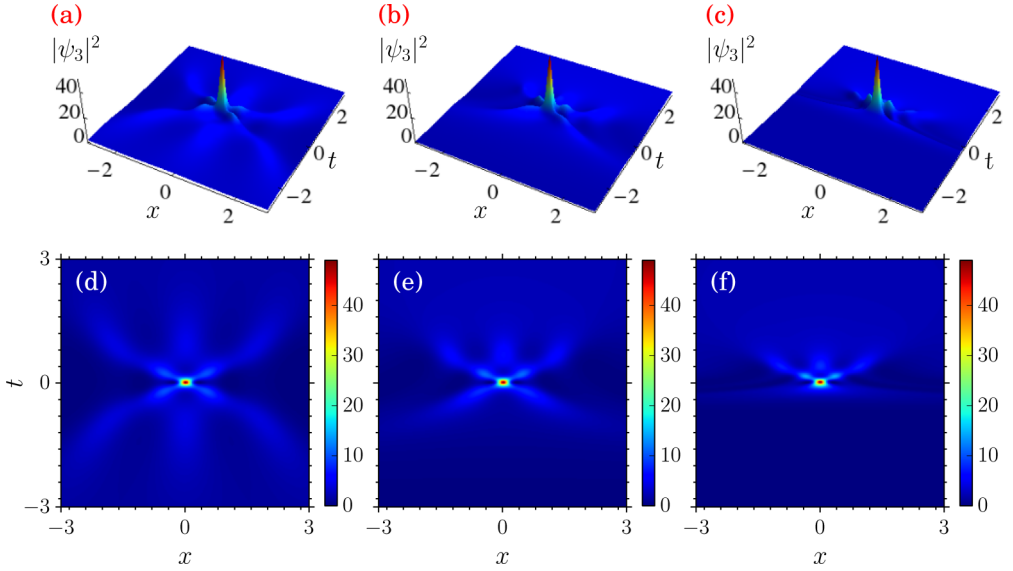

FIG. 9. (Color online) Third-order RWs for $R(t) = 1 + \tanh(\beta_0 t/2)$ and $\beta(t)^2 = \beta_0^2/2[1 - \tanh(\beta_0 t/2)]$. The parameter β_0 is varied as (a) $\beta_0 = 0.1$, (b) $\beta_0 = 1.0$, and (c) $\beta_0 = 5.0$. Panels (d)–(f) are their corresponding contour plots. The other parameters are the same as in Fig. 4.

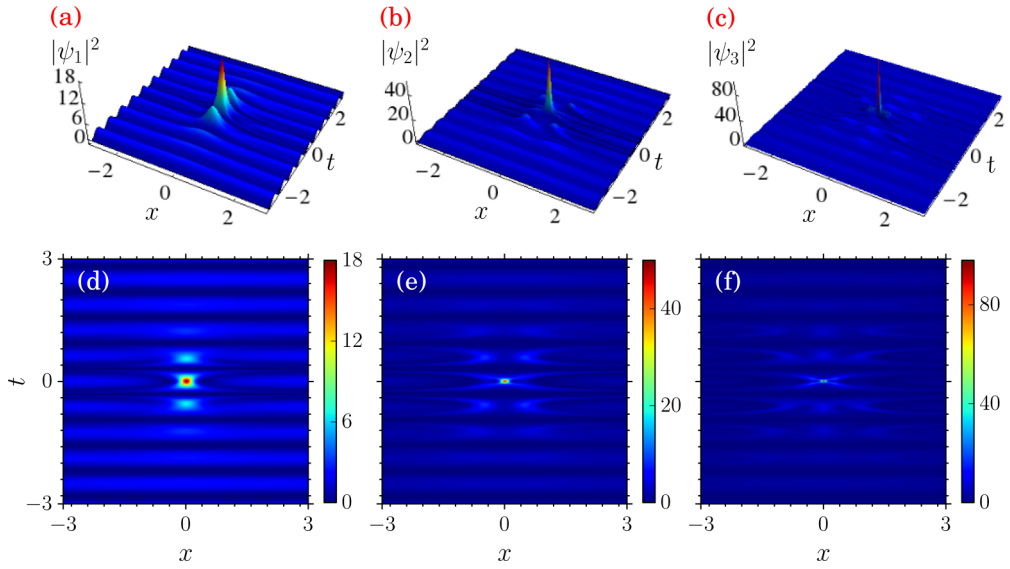

FIG. 10. (Color online) (a) First-order RW, (b) second-order RW, and (c) third-order RW for $R(t) = 1 + \cos(2\beta_0 t)$ and $\beta(t)^2 = 2\beta_0^2[1 + 3\tan^2(\beta_0 t)]$. Panels (d)–(f) are the corresponding contour plots of (a)–(c). The parameters are $r_0 = 1.0$, $\beta_0 = 2.5$, $c_1 = 0.01$, and $\delta = 0.01$.

Here $U_j(X,T)$, $j = 1,2,3$, are again the first-, second-, and third-order RW solutions of the NLS equation [see Eqs. (A2), (A4), and (A5)].

In Fig. 10 we present the density profiles of the first-, second-, and third-order RWs (first row) and their corresponding contour plots (second row) for the strength of time-dependent interatomic interaction $R(t) = 1 + \cos(2\beta_0 t)$ and time-dependent periodic trap frequency $\beta(t)^2 = 2\beta_0^2[1 + 3\tan^2(\beta_0 t)]$. Fixing the value of β_0 at 2.5, from Fig. 10 we see that the RW exists on a periodic background for the above forms of $R(t)$ and $\beta^2(t)$. Further we have also verified that the behavior of the RWs as a function of β_0 follows the same qualitative picture discussed above for the other forms of $R(t)$ and $\beta^2(t)$.

III. CHARACTERISTICS OF TRIPLET RWS

Very recently it has been shown that one can generalize the expressions for the higher-order RW solutions of the scalar NLS equation (2) given in Appendix further by introducing certain free parameters which allow one to split a symmetric form RW solution into a multipeaked solution and that by varying these free parameters one can extract certain novel patterns of RWs [44]. The introduction of free parameters decompose the higher-order RW solutions into $n(n+1)/2$ first-order forms, where n is the order of the RW, however, maintaining the symmetry of the higher-order solutions even in their decomposed forms. Further the free parameters are shown to determine the size and orientation of the first-order solutions [44]. Triplets are symmetry preserving first-order structures revealing the fact that the (higher-) second-order RW solution is a family of three first-order rational solutions. It is evident that the existence of triplets in an ocean corresponds to three big waves on the water surface in a row or "three sister waves" [45]. Inspired by such a possibility, in the following, we consider the second- and third-order RW solutions of (1) with suitable free parameters and analyze the symmetrical structures that arise due to these free parameters when we vary the strength of nonlinearity and the trap parameter. To begin with, we confine our attention to the second-order RW solution. In this case we have the following modified expressions [44] for G_2, H_2, and D_2 in Eq. (A3):

$$\begin{aligned} G_2 &= 12[3 - 16X^4 - 24X^2(4T^2+1) - 48lX - 80T^4 \\ &\quad - 72T^2 - 48mT], \\ H_2 &= 24\{T[15 - 16X^4 + 24X^2 - 48lX - 8(1-4X^2)T^2 \\ &\quad - 16T^4] + 6m(1 - 4T^2 + 4X^2)\}, \\ D_2 &= 64X^6 + 48X^4(4T^2+1) + 12X^2(3-4T^2)^2 + 64T^6 \\ &\quad + 432T^4 + 396T^2 + 9 + 48m[18m + T(9 + 4T^2 \\ &\quad - 12X^2)] + 48l[(18l + X(3 + 12T^2 - 4X^2)]. \end{aligned} \tag{12}$$

Note that this RW solution now contains two free parameters, l and m. The parameters l and m describe the relative positions of the first-order RWs in the triplet. Substituting the above expressions in Eqs. (9)–(11), for $j = 2$, we obtain the corresponding second-order RW solutions to the GP equation (1) with the free parameters l and m included. When $l = m = 0$, this solution coincides with the one given earlier [see Eq. (A4)], which contains one largest crest and four subcrests with two deepest troughs [Fig. 2(h)]. When l and m are not equal to 0, the second-order RW splits into three first-order RWs. These waves emerge in a triangular fashion (a triplet pattern). The three first-order RWs form a triangular pattern with 120 degrees of angular separation between them [44]. In Figs. 11(a)–11(c) we display the triplet pattern for $R(t) = \mathrm{sech}(\beta_0 t + \delta)$ and $\beta(t)^2 = \beta_0^2$ when $l = 15$ and $m = 25$. The triplet RW pattern for $\beta_0 = 0.1$ is shown in Fig. 11(a). When we increase the parameter β_0 to 0.3 we observe that the triplet pattern has started to collapse as shown in Fig. 11(b), and a complete collapse is observed as in Fig. 11(c) when we increase the β_0 value further to 1.0. Figures 11(d)–11(g) represent the triplet pattern for

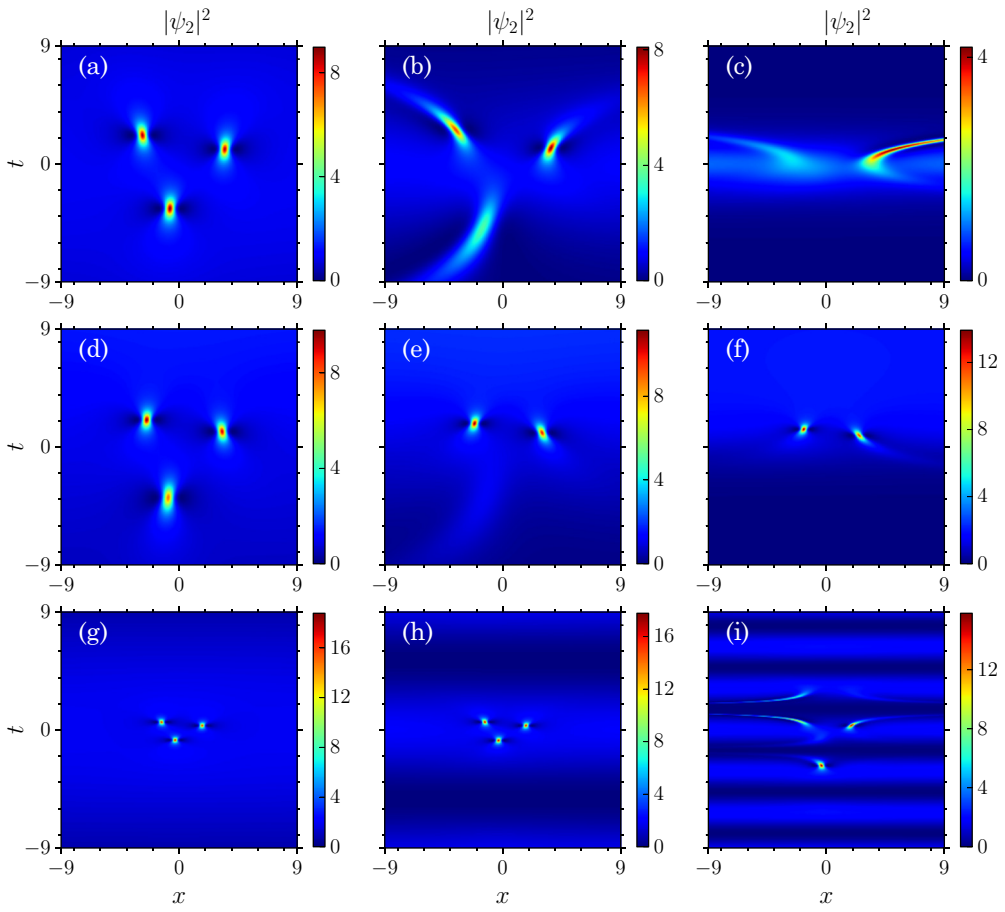

FIG. 11. (Color online) Triplet RWs. (a)–(c) $R(t) = \mathrm{sech}(\beta_0 t + \delta)$ and $\beta(t)^2 = \beta_0^2$; (d)–(f) $R(t) = 1 + \tanh(\beta_0 t/2)$ and $\beta(t)^2 = \beta_0^2/2[1 - \tanh(\beta_0 t/2)]$; (g)–(i) $R(t) = 1 + \cos(2\beta_0 t)$ and $\beta(t)^2 = 2\beta_0^2[1 + 3\tan^2(\beta_0 t)]$. Further, in (a), (d), and (g) $\beta_0 = 0.1$, in (b), (e), and (h) $\beta_0 = 0.3$, and in (c), (f), and (i) $\beta_0 = 1.0$. The other parameters are $l = 15$, $m = 25$, $r_0 = 1.0$, $c_1 = 0.01$, and $\delta = 0.01$.

$R(t) = 1 + \tanh(\beta_0 t/2)$ and $\beta(t)^2 = \beta_0^2/2[1 - \tanh(\beta_0 t/2)]$. The formation of triplet RWs is shown in Fig. 11(d) when $\beta_0 = 0.1$. When we increase the value β_0 to 0.3 one of the single RWs in the triplet pattern vanishes, which is illustrated in Fig. 11(e). By increasing the parameter β_0 further we observe that two first-order RWs are more localized in time, as shown in Fig. 11(f). Figures 11(g)–11(i) represent the triplet pattern for $R(t) = 1 + \cos(2\beta_0 t)$ and $\beta(t)^2 = 2\beta_0^2[1 + 3\tan^2(\beta_0 t)]$. The form of the triplet pattern for $\beta_0 = 0.1$ is displayed in Fig. 11(g). Here also when we increase the value of β_0 we observe the collapse of the triplet pattern in the periodic wave background [see Fig. 11(i)].

We then move on to investigate the structure of the third-order RW solution with four free parameters, l, m, g, and h. The third-order RW solution with four free parameters is much lengthier than the one without free parameters, and so we do not give the explicit expression here and analyze the results only graphically. Here also we analyze the solution with respect to the free parameters. When $l = m = g = h = 0$, we have the classical third-order RW solution, which is shown in Fig. 2(l). It has one largest crest and six subcrests with the two deepest troughs. For nonzero values of l, m, g, and h, the third-order RW splits into six separated first-order RWs. When we increase the value of the free parameters, the six first-order RWs take new positions. The sextet pattern is displayed in Figs. 12(a)–12(c) for $R(t) = \mathrm{sech}(\beta_0 t + \delta)$ and $\beta(t)^2 = \beta_0^2$ when $l = 10$, $m = 20$, $g = 500$, and $h = 500$. For $\beta_0 = 0.1$ the set of six first-order RWs is shown in Fig. 12(a). When we increase the value of β_0 to 0.25, three peaks disappear, and the remaining peaks start to bend as shown in Fig. 12(b). When we increase the value of β_0 further the RWs bend in the plane wave background as given in Fig. 12(c). Figures 12(d)–12(f) represent six first-order RWs for the time-dependent nonlinearity strength $R(t) = 1 + \tanh(\beta_0 t/2)$ and the time-dependent external trap frequency $\beta(t)^2 = \beta_0^2/2[1 - \tanh(\beta_0 t/2)]$. The formation of six first-order RWs at $\beta_0 = 0.1$ is shown in Fig. 12(d). When we increase the strength of the parameter β_0 to 0.25, one of six first-order RWs vanishes, as seen in Fig. 12(e). If we increase the value β_0 further, three out of six peaks bend in the plane wave background and eventually collapse, which is shown in Fig. 12(f). Figures 12(g)–12(i) represent the sextet pattern for $R(t) = 1 + \cos(2\beta_0 t)$ and $\beta(t)^2 = 2\beta_0^2[1 + 3\tan^2(\beta_0 t)]$. The form of the six first-order RWs for $\beta_0 = 0.05$ is displayed in Fig. 12(g), and for the further increase in β_0, the modified structures in the periodic wave background are as shown in Figs. 12(h) and 12(i).

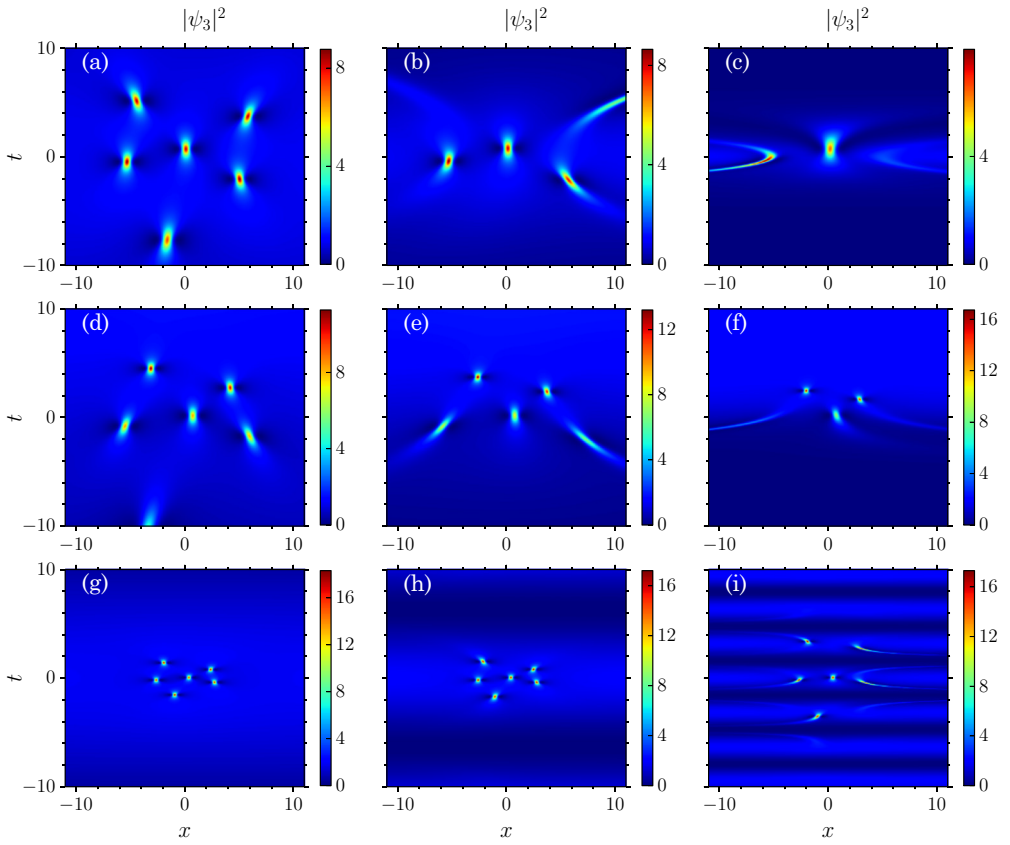

FIG. 12. (Color online) Sextet RWs. (a)–(c) $R(t) = \mathrm{sech}(\beta_0 t + \delta)$ and $\beta(t)^2 = \beta_0^2$; (d)–(f) $R(t) = 1 + \tanh(\beta_0 t/2)$ and $\beta(t)^2 = \beta_0^2/2[1 - \tanh(\beta_0 t/2)]$; (g)–(i) $R(t) = 1 + \cos(2\beta_0 t)$ and $\beta(t)^2 = 2\beta_0^2[1 + 3\tan^2(\beta_0 t)]$. Further, in (a), (d), and (g) $\beta_0 = 0.1$; in (b), (e), and (h) $\beta_0 = 0.25$; and in (c), (f), and (i) $\beta_0 = 1.0$. The other parameters are $l = 10$, $m = 20$, $g = 500$, $h = 500$, $r_0 = 1.0$, $c_1 = 0.01$, and $\delta = 0.01$.

IV. CHARACTERISTICS OF BREATHERS

In the previous two sections we have analyzed how the RW profiles get modified by the variations of the distributed coefficients present in the variable coefficient NLS equation (1). In this section we analyze how the breather structures get modified in the condensates when we vary the strength of the external trap parameter.

To begin, we consider the first-order breather solution of the NLS equation (2), which is given in Ref. [46] and is a special case of the GB solution (4),

$$\tilde{U}_1(X,T) = \left\{ \frac{f^2 \cosh[\alpha(T - T_1)] + 2i\, f v \sinh[\alpha(T - T_1)]}{2\cosh[\alpha(T - T_1)] - 2v\cos[f(X - X_1)]} - 1 \right\} \times \exp(iT), \tag{13}$$

where the parameters f and v are expressed in terms of a complex eigenvalue (e.g., λ), that is, $f = 2\sqrt{1 + \lambda^2}$ and $v = \mathrm{Im}(\lambda)$, and X_1 and T_1 serve as coordinate shifts from the origin. The real part of the eigenvalue represents the angle that the one-dimensionally localized solutions form with the T axis, and the imaginary part characterizes frequency of periodic modulation. The parameter α $(= f v)$ in Eq. (13) is the growth rate of modulation instability. Substituting this breather solution of the NLS equation into (9)–(11), we study the underlying dynamics of (1).

For illustration, we consider the case $R(t) = \mathrm{sech}(\beta_0 t + \delta)$ and $\beta(t)^2 = \beta_0^2$ and plot the outcome in Fig. 13. The first row in Fig. 13 represents an Akhmediev breather (AB) solution for the eigenvalue $\lambda = 0.6i$ and Ma breather (MB) solution

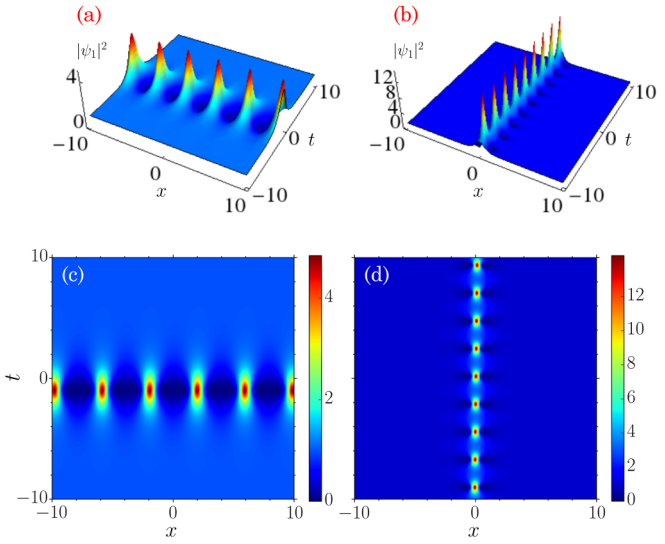

FIG. 13. (Color online) (a) AB for $\lambda = 0.6i$, (b) MB for $\lambda = 1.4i$ when $R(t) = \mathrm{sech}(\beta_0 t + \delta)$ and $\beta(t)^2 = \beta_0^2$. (c) and (d) Their corresponding contour plots. The other parameters are $r_0 = 1.0$, $\beta_0 = 0.01$, $c_1 = 0.01$, and $\delta = 0.01$.

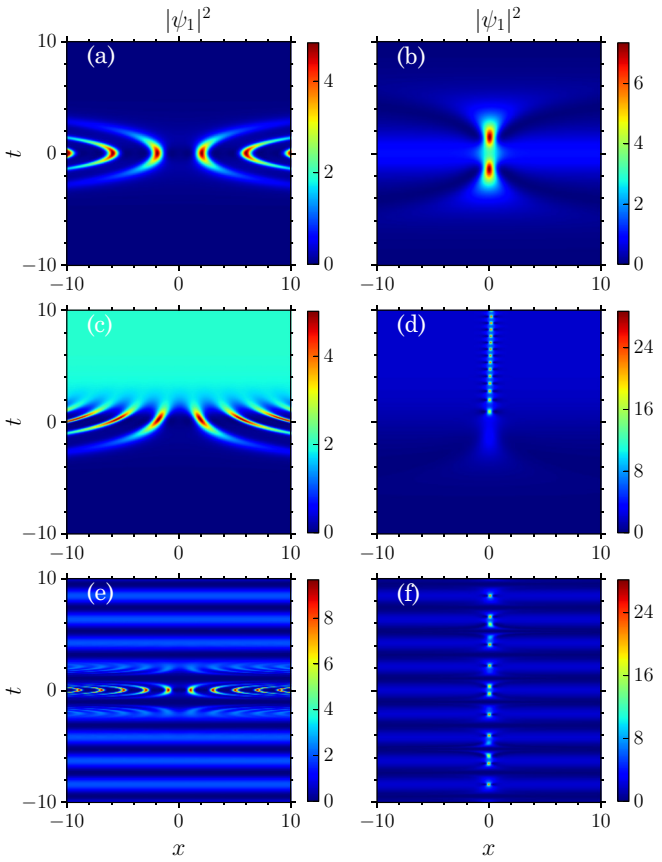

FIG. 14. (Color online) Stretching of breathers. (a), (c), and (e) AB with an eigenvalue $\lambda = 0.6i$; (b), (d), and (f) MB with $\lambda = 1.4i$ for the three different forms of $R(t)$ discussed in the text. (a)–(d) $\beta_0 = 0.8$, (e) and (f) $\beta_0 = 1.5$. The other parameters are $r_0 = 1.0$, $c_1 = 0.01$, and $\delta = 0.01$.

for $\lambda = 1.4i$, and the second row represents their contour plots. The AB and MB solutions are localized in time and space, respectively, as discussed in Sec. I. This is clearly demonstrated in the two columns of Fig. 13. When we tune the parameter β_0, a new structure against a breather background is obtained. To visualize this we fix the value of β_0 to be 0.8. For this value a stretching occurs in space in the case of AB [Fig. 14(a)], whereas in the case of MB [Fig. 14(b)] the stretching occurs in time. Figures 14(c)–14(d) illustrate the AB and MB profiles for the time-dependent nonlinearity coefficient $R(t) = 1 + \tanh(\beta_0 t/2)$ and time-dependent trap frequency $\beta(t)^2 = (\beta_0^2/2)[1 - \tanh(\beta_0 t/2)]$. Here also we tune the strength of the trap parameter β_0 to 0.8 and observe that stretching occurs over space in AB, which is depicted in Fig. 14(c), and the MB gets more localized, and when $t \leqslant 0$ the breather profile completely disappears, as shown in Fig. 14(d). Our results reveal the fact that when we tune the parameter β_0 in the obtained breather solution, the breather gets a modified structure corresponding to a distortion of the breather profile. Figures 14(e) and 14(f), respectively, represent the AB and MB in the periodic background for $R(t) = 1 + \cos(2\beta_0 t)$ and $\beta(t)^2 = 2\beta_0^2[1 + 3\tan^2(\beta_0 t)]$ when $\beta_0 = 1.5$.

Next, we proceed to construct the two-breather solutions of (1) and analyze how these solutions are distorted by the variations of modulation parameters. The two-breather solution of the NLS equation is given by [47]

$$\tilde{U}_2(X,T) = \left[1 + \frac{\tilde{G}_2(X,T) + i\tilde{H}_2(X,T)}{\tilde{D}_2(X,T)}\right]\exp(iT), \quad (14)$$

where $\tilde{G}_2$, $\tilde{H}_2$, and $\tilde{D}_2$ are given by

$$\begin{aligned}\tilde{G}_2 = &-\left(k_1^2 - k_2^2\right)\left[\frac{k_1^2\delta_2}{k_2}\cosh(\delta_1 T_{s1})\cos(k_2 X_{s2})\right.\\ &-\left(k_1^2 - k_2^2\right)\cosh(\delta_1 T_{s1})\cosh(\delta_2 T_{s2})\\ &\left.-\frac{k_2^2\delta_1}{k_1}\cosh(\delta_2 T_{s2})\cos(k_1 X_{s1})\right], \quad (15a)\end{aligned}$$

$$\begin{aligned}\tilde{H}_2 = &-2\left(k_1^2 - k_2^2\right)\left[\frac{\delta_1\delta_2}{k_2}\sinh(\delta_1 T_{s1})\cos(k_2 X_{s2})\right.\\ &-\frac{\delta_1\delta_2}{k_1}\sinh(\delta_2 T_{s2})\cos(k_1 X_{s1})\\ &-\delta_1\sinh(\delta_1 T_{s1})\cosh(\delta_2 T_{s2})\\ &\left.+\delta_2\sinh(\delta_2 T_{s2})\cosh(\delta_1 T_{s1})\right], \quad (15b)\end{aligned}$$

$$\begin{aligned}\tilde{D}_2 = &\,2\left(k_1^2 + k_2^2\right)\frac{\delta_1\delta_2}{k_1 k_2}\cos(k_1 X_{s1})\cos(k_2 X_{s2})\\ &+4\delta_1\delta_2(\sin(k_1 X_{s1})\sin(k_2 X_{s2})\\ &+\sinh(\delta_1 T_{s1})\sinh(\delta_2 T_{s2}))\\ &-\left(2k_1^2 - k_1^2 k_2^2 + 2k_2^2\right)\cosh(\delta_1 T_{s1})\cosh(\delta_2 T_{s2})\\ &-2\left(k_1^2 - k_2^2\right)\left[\frac{\delta_1}{k_1}\cos(k_1 X_{s1})\cosh(\delta_2 T_{s2})\right.\\ &\left.-\frac{\delta_2}{k_2}\cos(k_2 X_{s2})\cosh(\delta_1 T_{s1})\right], \quad (15c)\end{aligned}$$

where the modulation frequencies, $k_j = 2\sqrt{1+\lambda_j^2}$, $j = 1,2$, are described by the (imaginary) eigenvalues λ_j. In the above expressions, X_j, T_j, $j = 1,2$, represent the shifted point of origin, δ_j $(=k_j\sqrt{4-k_j^2}/2)$ is the instability growth rate of each component, and $X_{sj} = X - X_j$ and $T_{sj} = T - T_j$ are shifted variables.

With two purely imaginary eigenvalues, λ_j, $j = 1,2$, solution (14) is capable of describing a variety of possible second-order breather structures. The solution includes ABs, MBs, and the intersection of AB and MB solutions for certain combinations of eigenvalues. For example, when the imaginary parts of both eigenvalues $\mathrm{Im}(\lambda_j)$, $j = 1,2$, lie between 0 and 1, we obtain the ABs. On the other hand, when both of them are greater than one $[\mathrm{Im}(\lambda_j) > 1]$ we obtain the MBs, and in the mixed possibility case, that is, one of the eigenvalues is less than one $[\mathrm{Im}(\lambda_1) < 1]$ and the other eigenvalue $[\mathrm{Im}(\lambda_2) > 1)$ is greater than one, we obtain the intersection of AB and MB solutions.

Substituting the two-breather NLS solution (14) in Eqs. (9)–(11) we obtain the general two-breather solution of (1). Figure 15 displays the evolution of the two-breather solution of (1) for $R(t) = \mathrm{sech}(\beta_0 t + \delta)$ and $\beta(t)^2 = \beta_0^2 = (0.01)^2$ with imaginary eigenvalues. To obtain the ABs from (14) we consider the situation where the magnitudes of both eigenvalues

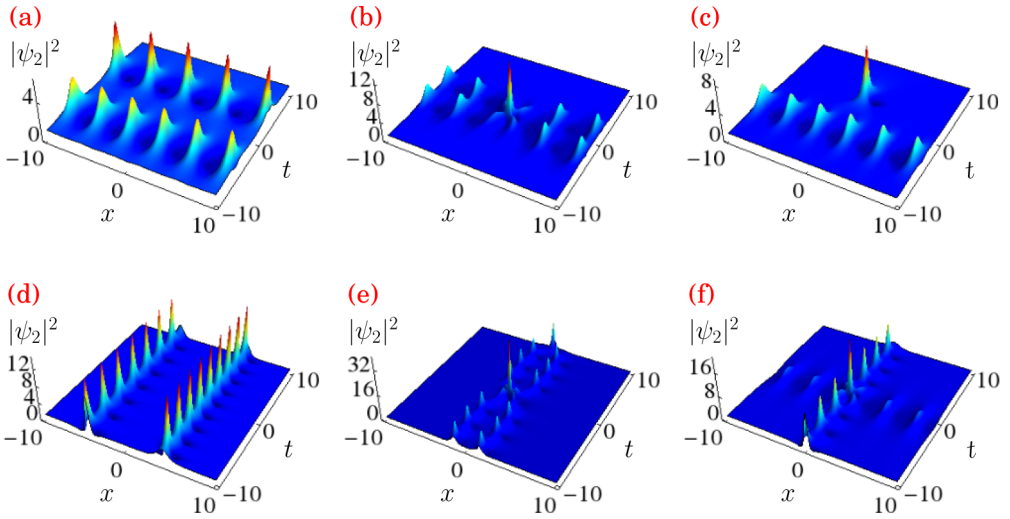

FIG. 15. (Color online) (a) Two AB profiles for $\lambda_1 = 0.55i$ and $\lambda_2 = 0.75i$ with $T_1 = -3$ and $T_2 = 3$. (b) Two ABs without time shifts. (c) AB-RW profile for $\lambda_1 = 0.55i$ and $\lambda_2 = 0.99i$. (d) Two MBs for $\lambda_1 = 1.3i$ and $\lambda_2 = 1.4i$ with $X_1 = -3$ and $X_2 = 3$. (e) Two MBs without space shifts and (f) the intersection of AB and MB for $\lambda_1 = 0.5i$ and $\lambda_2 = 1.3i$ for $R(t) = \mathrm{sech}(\beta_0 t + \delta)$ and $\beta(t)^2 = \beta_0^2$. The other parameters are the same as in Fig. 4.

λ_1 and λ_2 are less than 1 ($\lambda_1 = 0.55i$ and $\lambda_2 = 0.75i$). One AB developing with a time delay after another is shown in Fig. 15(a), while in Fig. 15(b) we present the case where there is no such time delay. In Fig. 15(c) we depict the case when one AB along with a RW coexist for the choice $\lambda_1 = 0.55i$ and $\lambda_2 = 0.99i$. When we take the eigenvalues λ_1 and λ_2 to be $1.3i$ and $1.4i$, respectively, we obtain two MB solutions. Similarly the evolution of the two MBs with and without spatial

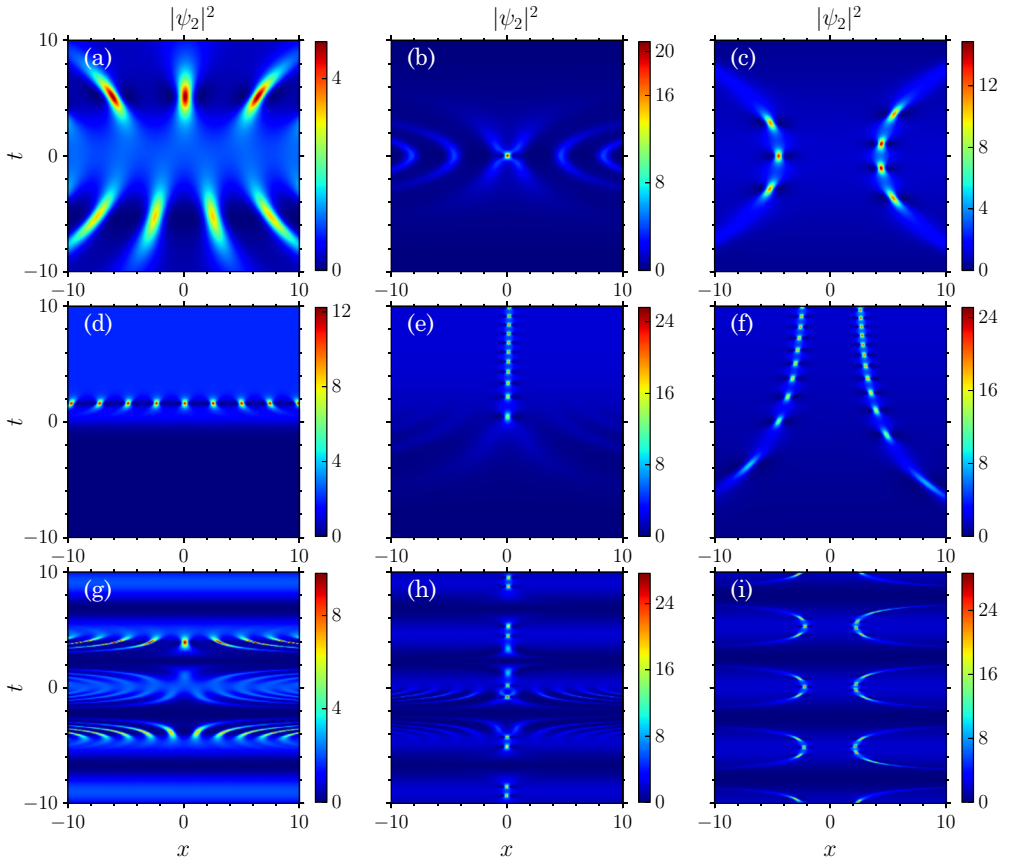

FIG. 16. (Color online) Distortion of two-breather profiles. (a), (d), and (g) Two ABs with $\lambda_1 = 0.55i$ and $\lambda_2 = 0.75i$; (b), (e), and (h) the intersection of AB-MB profiles with $\lambda_1 = 0.5i$ and $\lambda_2 = 1.3i$; and (c), (f), and (i) two MBs with $\lambda_1 = 1.3i$ and $\lambda_2 = 1.4i$. The trap parameter β_0 is chosen as (a) 0.15, (b), and (e) 0.5, (c) and (f) 0.2, (d) 1.5 and (g)–(i) 0.7. The other parameters are $r_0 = 1.0$, $c_1 = 0.01$, and $\delta = 0.01$.

delay is shown in Figs. 15(d) and 15(e), respectively. We also observe that the distance between the MBs increases when we set both eigenvalues to be nearly equal, for example, $\lambda_1 = 1.3i$ and $\lambda_2 = 1.31i$, which is not displayed here. When we take the eigenvalues as $\lambda_1 = 0.5i$ and $\lambda_2 = 1.3i$, the AB intersects with the MB, which is displayed in Fig. 15(f). When we tune the strength of the trap parameter β_0 to 0.15, both ABs get stretched in the plane wave background, which is demonstrated in Fig. 16(a). When $\beta_0 = 0.5$, in the intersection of AB and MB solutions we observe that the AB gets a bending structure while the MB fully disappears in the plane wave background, which is shown in Fig. 16(b). In Fig. 16(c) we note that both MBs develop a bending structure in the plane wave background when $\beta_0 = 0.2$. Figures 16(d)–16(f) display the evolution of the two-breather solution of (1) for $R(t) = 1 + \tanh(\beta_0 t/2)$ and $\beta(t)^2 = \beta_0^2/2[1 - \tanh(\beta_0 t/2)]$ with the imaginary eigenvalues. When $\beta_0 = 0.15$ one of the ABs gets stretched, which is not shown here, and on further increase of the value of β_0 to 1.5, one of the ABs gets annihilated and the other AB bends in the plane wave background, which is demonstrated in Fig. 16(d). When $\beta_0 = 0.5$ the intersection of AB-MB structures is as shown in Fig. 16(e). In Fig. 16(f) we observe that both MBs get a bending structure in the plane wave background. Figures 16(g)–16(i) show the evolution of the two-breather solution of (1) for $R(t) = 1 + \cos(2\beta_0 t)$ and $\beta(t)^2 = 2\beta_0^2[1 + 3\tan^2(\beta_0 t)]$ with the imaginary eigenvalues. Here also when we increase the value of β_0 we observe the collapse of the two-breather solution in the periodic wave background.

V. CONCLUSION

In this work, we have constructed higher-order RW solutions with and without free parameters for the quasi-one-dimensional GP equation with time-dependent interatomic interaction and an external trap through the similarity transformation technique. By mapping the variable coefficient NLS equation onto the constant coefficient NLS equation we have derived these solutions. We have shown that the mapping can be done when the external trap and the nonlinearly interatomic interaction of atoms satisfy a constraint. From the known higher-order RW and breather solutions of the constant coefficient NLS equation, we have derived the solutions of (1). In our analysis, we have considered the harmonic trap frequency in three different forms: (i) the time-independent expulsive trap, (ii) time-dependent monotonous trap, and (iii) time-dependent periodic trap, and correspondingly fixed the effective scattering length. We then studied the characteristics of the constructed RW solutions in detail. We have observed that the second- and third-order RWs transform to first-order RW-like structures when a parameter appearing in the harmonic trap (time-independent and time-dependent traps) is varied. We have then analyzed the characteristics of triplet and sextet patterns of matter RWs for (1). We have also constructed one-breather and two breather solutions of (1). We have investigated how these periodic localized waves change in the plane wave background when we tune the trap parameter in the obtained breather solutions. Our results may provide possibilities to manipulate RWs experimentally in a BEC system.

ACKNOWLEDGMENTS

K.M. thanks the University Grants Commission (UGC-RFSMS), Government of India, for providing a research fellowship. The work of P.M. forms part of the Department of Science and Technology (Ref. No. SR/S2/HEP-03/2009) and Council of Scientific and Industrial Research (Ref. No. 03(1186)/10/EMR-II), Government of India-funded research projects. The work of M.S. forms part of a research project sponsored by NBHM, Government of India. The work forms part of an IRHPA project and a Ramanna Fellowship project of M.L., sponsored by the Department of Science and Technology (DST), Government of India, and he is also supported by a DAE Raja Ramanna Fellowship.

APPENDIX

In the absence of the trap, and the nonlinearity strength $R(t)$ is equal to one, Eq. (1) reduces to the standard NLS equation (2). Several localized and periodic structures of standard NLS are documented in the literature [21,46,47]. Equation (2) admits an Nth-order RW solution. We present the RW solution of the NLS equation in the following form [21]:

$$U_j(X,T) = \left[(-1)^j + \frac{G_j(X,T) + iTH_j(X,T)}{D_j(X,T)}\right]\exp(iT), \tag{A1}$$

where $j = 1,2,\ldots,G_j,H_j$, and D_j are polynomials in the variables T and X.

For the first-order ($j = 1$) RW solution $G_1 = 4$, $H_1 = 8$, and $D_1 = 1 + 4X^2 + 4T^2$. From (A1) we get $U_1 = (4\frac{1+2iT}{1+4X^2+4T^2} - 1)\exp(iT)$. For convenience we multiply this expression by $-1 = \exp[i\pi]$ and consider the solution in the form

$$U_1(X,T) = \left(1 - 4\frac{1+2iT}{1+4X^2+4T^2}\right)\exp[iT]. \tag{A2}$$

We use only this form of expression in our analysis. This solution is same as the one given in Eq. (5) when $k = 0, \omega = 1$ and $\rho_0 = 1$. For the second-order ($j = 2$) RW solution, the function G_2, H_2, and D_2 turn out to be [21]

$$\begin{aligned} G_2 &= \tfrac{3}{8} - 3X^2 - 2X^4 - 9T^2 - 10T^4 - 12X^2T^2, \\ H_2 &= \tfrac{15}{4} + 6X^2 - 4X^4 - 2T^2 - 4T^4 - 8X^2T^2 \end{aligned} \tag{A3}$$

and

$$\begin{aligned} D_2 = \tfrac{1}{8}\big(&\tfrac{3}{4} + 9X^2 + 4X^4 + \tfrac{16}{3}X^6 + 33T^2 + 36T^4 \\ &+ \tfrac{16}{3}T^6 - 24X^2T^2 + 16X^4T^2 + 16X^2T^4\big). \end{aligned}$$

Then we get

$$U_2(X,T) = \left[1 + \frac{G_2 + iTH_2}{D_2}\right]\exp(iT). \tag{A4}$$

The profiles of second-order RW and third-order RW of the constant coefficient NLS equation are shown in Fig. 17. For

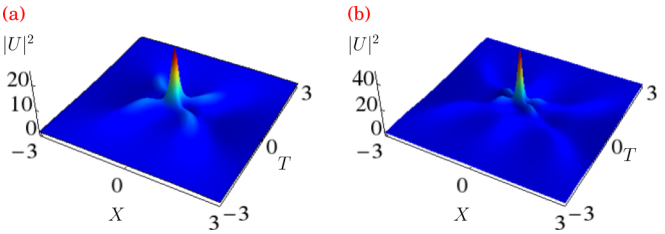

FIG. 17. (Color online) Profiles: (a) Second-order RW and (b) third-order RW of the standard NLS equation.

the third-order ($j = 3$) RW solution, we have

$$U_3(X,T) = \left[-1 + \frac{G_3 + iTH_3}{D_3} \right] \exp(iT), \tag{A5}$$

where

$$G_3(X,T) = g_0 + (2T)^2 g_2 + (2T)^4 g_4 + (2T)^6 g_6 + (2T)^8 g_8 + (2T)^{10} g_{10}, \tag{A6}$$

with

$$\begin{aligned} g_0 &= 1 - (2X)^2 - \frac{2}{3}(2X)^4 + \frac{14}{45}(2X)^6 + \frac{(2X)^8}{45} + \frac{(2X)^{10}}{675}, \\ g_2 &= -3 - 20(2X)^2 + \frac{2}{3}(2X)^4 - \frac{4}{45}(2X)^6 + \frac{(2X)^8}{45}, \\ g_4 &= 2\left[-\frac{17}{3} + 5(2X)^2 - \frac{(2X)^4}{3^2} + \frac{(2X)^6}{3^3} \right], \\ g_6 &= \frac{2}{45}\left[73 + 14(2X)^2 + \frac{7}{3}(2X)^4 \right], \\ g_8 &= \frac{1}{15}(11 + (2X)^2), \quad g_{10} = \frac{11}{675} \end{aligned} \tag{A7}$$

and

$$H_3(X,T) = h_0 + (2T)^2 h_2 + (2T)^4 h_4 + (2T)^6 h_6 + (2T)^8 h_8 + (2T)^{10} h_{10}, \tag{A8}$$

with

$$\begin{aligned} h_0 &= 2\left[7 + 7(2X)^2 - 2(2X)^4 - \frac{2}{3^2}(2X)^6 - \frac{(2X)^8}{45} + \frac{(2X)^{10}}{675} \right], \\ h_2 &= \frac{2}{3}\left[-11 - 28(2X)^2 - 2(2X)^4 - \frac{28}{45}(2X)^6 + \frac{(2X)^8}{45} \right], \\ h_4 &= \frac{4}{15}\left[-107 + 19(2X)^2 - \frac{7}{3}(2X)^4 + \frac{(2X)^6}{3^2} \right], \\ h_6 &= \frac{4}{45}\left[-29 - 2(2X)^2 + \frac{(2X)^4}{3} \right], \\ h_8 &= \frac{2}{3^3}\left[1 + \frac{(2X)^2}{5} \right], \quad h_{10} = \frac{2}{675}. \end{aligned} \tag{A9}$$

The denominator is represented by

$$D_3(X,T) = d_0 + (2T)^2 d_2 + (2T)^4 d_4 + (2T)^6 d_6 + (2T)^8 d_8 + (2T)^{10} d_{10} + (2T)^{12} d_{12}, \tag{A10}$$

where

$$\begin{aligned} d_0 &= \frac{1}{2^3}\left[1 + 6(2X)^2 + \frac{5}{3}(2X)^4 + \frac{52}{45}(2X)^6 + \frac{(2X)^8}{15} + \frac{2}{675}(2X)^{10} + \frac{(2X)^{12}}{2025} \right], \\ d_2 &= 23 - 9(2X)^2 + \frac{10}{3}(2X)^4 + \frac{2}{15}(2X)^6 - \frac{(2X)^8}{45} + \frac{(2X)^{10}}{675}, \\ d_4 &= 2\left[71 + \frac{116}{3}(2X)^2 - \frac{2}{3}(2X)^4 - \frac{4}{45}(2X)^6 + \frac{(2X)^8}{135} \right], \\ d_6 &= \frac{32}{3}\left[\frac{17}{3} + 5(2X)^2 + \frac{(2X)^4}{45} + \frac{(2X)^6}{135} \right], \\ d_8 &= \frac{32}{15}\left[\frac{83}{3} + 2(2X)^2 + \frac{(2X)^4}{3^2} \right], \\ d_{10} &= \frac{2^8}{225}\left[7 + \frac{(2X)^2}{3} \right], \quad d_{12} = \frac{2^9}{2025}. \end{aligned} \tag{A11}$$

[1] S. Ponomarenko and G. P. Agrawal, Phys. Rev. Lett. **97**, 013901 (2006).

[2] V. N. Serkin, A. Hasegawa, and T. L. Belyaeva, Phys. Rev. Lett. **98**, 074102 (2007).

[3] M. Centurion, M. A. Porter, P. G. Kevrekidis, and D. Psaltis, Phys. Rev. Lett. **97**, 033903 (2006).

[4] A. Hasegawa and M. Matsumoto, *Optical Solitons in Fibers* (Springer, Berlin, 2003).

[5] D. R. Solli, C. Ropers, P. Koonath, and B. Jalali, Nature (London) **450**, 1054 (2007).

[6] C. J. Pethick and H. Smith, *Bose-Einstein Condensation in Dilute Gases* (Cambridge University Press, Cambridge, 2008).

[7] F. Dalfovo, S. Giorgini, L. P. Pitaevskii, and S. Stringari, Rev. Mod. Phys. **71**, 463 (1999).

[8] R. Carretero-Gonzalez, D. J. Frantzeskakis, and P. G. Kevrekidis, Nonlinearity **21**, R139 (2008).

[9] L. Pitaevskii and S. Stringari, *Bose-Einstein Condensation* (Oxford University Press, New York, 2003).

[10] V. M. Perez-Garcia, H. Michinel, and H. Herrero, Phys. Rev. A **57**, 3837 (1998).

[11] S. Rajendran, P. Muruganandam, and M. Lakshmanan, Physica D **239**, 366 (2010).
[12] R. Atre, P. K. Panigrahi, and G. S. Agarwal, Phys. Rev. E **73**, 056611 (2006).
[13] M. Lakshmanan and S. Rajasekar, *Nonlinear Dynamics: Integrablity, Chaos and Patterns* (Springer-Verlag, Heidelberg, 2003).
[14] D. Mandelik, H. S. Eisenberg, Y. Silberberg, R. Morandotti, and J. S. Aitchison, Phys. Rev. Lett. **90**, 253902 (2003).
[15] M. Tajiri and Y. Watanabe, Phys. Rev. E **57**, 3510 (1998).
[16] D. H. Pergrine, J. Austral. Math. Soc. Ser. B **25**, 16 (1983).
[17] A. R. Osborne, M. Onorato, and M. Serio, Phys. Lett. A **275**, 386 (2000).
[18] A. R. Osborne, *Nonlinear Ocean Waves* (Academic Press, New York, 2009).
[19] C. Kharif, E. Pelinovsky, and A. Slunyaev, *Rogue Waves in the Ocean* (Springer-Verlag, Berlin, 2009).
[20] T. B. Benjamin and J. E. Feir, J. Fluid Mech. **27**, 417 (1967).
[21] N. Akhmediev, A. Ankiewicz, and J. M. Soto-Crespo, Phys. Rev. E **80**, 026601 (2009).
[22] A. Chabchoub, N. P. Hoffmann, and N. Akhmediev, Phys. Rev. Lett. **106**, 204502 (2011).
[23] M. Shats, H. Punzmann, and H. Xia, Phys. Rev. Lett. **104**, 104503 (2010).
[24] B. Kibler, J. Fatome, C. Finot, F. Dias, G. Genty. N. Akhmediev, and J. M. Dudley, Nat. Phys. **6**, 790 (2010).
[25] J. He, S. Hu, and K. Porsezian, Phys. Rev. E **86**, 066603 (2012).
[26] J. S. He, H. R. Zhang, L. H. Wang, K. Porsezian, and A. S. Fokas, Phys. Rev. E **87**, 052914 (2013).
[27] W. M. Moselem, Phys. Plasmas **18**, 032301 (2011).
[28] G. P. Veldas, J. Borhanian, M. Mckerr, V. Saxena, D. J. Frantzeskakis, and I. Kourakis, J. Optics. **15**, 064003 (2013).
[29] Z. Y. Yan, Commun. Theor. Phys. **54**, 947 (2010).
[30] K. Staliunas, S. Longhi, and G. J. deValcarcel, Phys. Rev. Lett. **89**, 210406 (2002).
[31] F. Kh. Abdullaev, J. G. Caputo, R. A. Kraenkel, and B. A. Malomed, Phys. Rev. A **67**, 013605 (2003).
[32] A. D. Cronin, J. Schmiedmayer, and D. E. Pritchard, Rev. Mod. Phys. **81**, 1051 (2009).
[33] O. Mandel, M. Greiner, A. Widera, T. Rom, T. H. Hänsch, and I. Bloch, Phys. Rev. Lett. **91**, 010407 (2003).
[34] J. I. Cirac and P. Zoller, Phys. Rev. Lett. **74**, 4091 (1995).
[35] Y. V. Bludov, V. V. Konotop, and N. Akhmediev, Phys. Rev. A **80**, 033610 (2009).
[36] Z. Y. Yan, Phys. Lett. A **374**, 672 (2010).
[37] L. Wen, L. Li, Z.-D. Li, S.-W. Song, X.-F. Zhang, and W. M. Liu, Eur. Phys. J. D **64**, 473 (2011).
[38] L. C. Zhao, Ann. Phys. **329**, 73 (2013)
[39] X. F. Wu, G. S. Hua, and Z. Y. Ma, Commun. Nonlinear Sci. Num. Simulat. **18**, 3325 (2013).
[40] J. S. He, E. G. Charalampidis, P. G. Kevrekidis, and D. J. Frantzeskakis, Phys. Lett. A **378**, 577 (2014).
[41] S. Rajendran, P. Muruganandam, and M. Lakshmanan, J. Phys. B **42**, 145307 (2009).
[42] C. Özemír and F. Güngor, Rev. Math. Phys. **24**, 1250015 (2012).
[43] P. Muruganandam and S. K. Adhikari, Comput. Phys. Commun. **180**, 1888 (2009); D. Vudragović, I. Vidanović, A. Balaž, P. Muruganandam, and S. K. Adhikari, *ibid.* **183**, 2021 (2012).
[44] A. Ankiewicz, D. J. Kedziora, and N. Akhmediev, Phy. Lett. A **375**, 2782 (2011).
[45] J. F. Wolff, *Lake Superior Shipwrecks* (Lake Superior Marine Museum Association, Duluth, MN, 1979), p. 28.
[46] N. Akhmediev, V. M. Eleonskii, and N. E. Kulagin, Zh. Eksperimentalnoii i Teoreticheskoii Fiziki **89**, 1542 (1985) [Sov. Phys. JETP **62**, 894 (1985)].
[47] D. J. Kedziora, A. Ankiewicz, and N. Akhmediev, Phys. Rev. E **85**, 066601 (2012).